Natural Phosphates Characterization and Evaluation of their Removal Efficiency of Methylene Blue and Methyl Orange from Aqueous Media

Meryem Assimeddine, Mohamed Abdennouri, Noureddine Barka, Rachid Elmoubarki, and M'hamed Sadiq*

Sultan Moulay Slimane University of Beni Mellal, Research Group in Environmental Sciences and Applied Materials (SEMA), FP Khouribga, B.P. 145, 25000, Morocco

ARTICLE INFO

Received: 5 Aug 2021
Received in revised: 30 Sep 2021
Accepted: 3 Oct 2021
Published online: 8 Oct 2021
DOI: 10.32526/ennrj/20/202100147

Keywords:
Natural phosphate/ Adsorption/ Methyl orange/ Methylene blue

*** Corresponding author:**
E-mail: m.sadiq@usms.ma

ABSTRACT

This study evaluated the capacity of a rock phosphate for the adsorption of organic dyes methylene blue MB and methyl orange MO in aqueous solution, in order to minimize the impact of these dyes on the environment. The physicochemical characterization of natural phosphates (NP) shows that its mineralogy is carbonate-fluorapatite, calcite and quartz, as demonstrated by X-ray diffraction. An infrared (IR) analysis completed the structural study by confirming the characteristic bands of a carbonated fluorapatite type B. The influence of adsorbent dose, pH, initial concentration and temperature of the dye solution on adsorption onto NP was studied. The experimental results show that MB is adsorbed almost entirely at an adsorbent dose of 1 g/L and at a more basic pH and that the Langmuir model describes its isotherm well. For MO, adsorption is performed at acidic pH, such that discoloration reaches 60% at pH 4 and NP adsorbent dose of 10 g/L. The maximum adsorbed amounts of MB (pH=9) and MO (pH=4) were found to be 9.54 and 1.09 mg/g, respectively. The kinetic data were analyzed to show that the pseudo-second-order model seems to be the most appropriate to describe the adsorption dynamics of both dyes on the naturel phosphate. The thermodynamic results show that the adsorption is endothermic for MB and exothermic for MO. So, rock phosphate shows a good potential as a sorbent for cationic dyes removal from wastewater.

1. INTRODUCTION

Currently, drinking water resources are greatly reduced due to an increase in population accompanied by intensive development of agriculture and strong industrialization. In addition, the discharge of wastewater into the natural environment from urban, rural, and industrial centers, without preliminary treatment, negatively impacts the quality of water resources. The garment and the textile industry are among the most demanding industries in the world in terms of water consumption and, therefore, discharge large amounts of wastewater charged in dyes. This industry uses chemicals, including dyes, which are generally responsible for many harmful environmental and health effects (Combes and Haveland-Smith, 1982; Chen, 2006; Tsuda et al., 2000; Heiss et al., 1992; Daneshvar et al., 2003) due to their complex synthetic nature, which makes them more stable and therefore not easily biodegradable (Damodar et al., 2007; Gupta and Khatri, 2019; Elmoubarki et al., 2015). The elimination of these effluents is one of the main problems in the treatment process of liquid waste. Several techniques such as chemical, physical, physicochemical and biological have been used to remove organic dyes. Their objective is to find a treatment process that is technically accessible and economically suitable for the industry. The adsorption technique is the most favorable method for removing organic dyes and has become an analytical method of choice, highly effective and simple to use (Sabar et al., 2020; Bedin et al., 2017). In addition, the use of a natural and abundant adsorbent for wastewater treatment is a legitimate way to preserve water capital (Bensalah et al., 2017; Assimeddine et al., 2020). Moroccan natural phosphates are mainly constituted by fluoroapatite $Ca_{10}(PO_4)_6F_2$ and partially substituted by carbonate. Due to their surface properties and multiple chemical components, they are widely used

Citation: Assimeddine M, Abdennouri M, Barka N, Elmoubarki R, Sadiq M. Natural phosphates characterization and evaluation of their removal efficiency of methylene blue and methyl orange from aqueous media. Environ. Nat. Resour. J. 2022;20(1):29-41. (https://doi.org/10.32526/ennrj/20/202100147)

as adsorbent for many physico-chemical processes. Among them, removal of methylene blue (MB), basic yellow 28 and reactive yellow 125 (Barka et al., 2009), elimination of cationic dye rhodamine 6G (Rh6G) as well as anionic dye congo red (CR) from wastewater (Bensalah et al., 2017) and removal of lead ions from aqueous solution (Mouflih et al., 2006). In order to broaden the scope and improve the previous research, the present work is based on the physico-chemical characterization of Moroccan naturel phosphate and the study of its capacity to decolorize wastewater. Methylene blue (MB) and methyl orange (MO) were chosen as dyes because they are among the most widely used in dyeing. They are also two model dyes for the evaluation of the adsorption capacity of adsorbents and have two different characters where MB is cationic dye and OM is anionic dye. In addition, these dyes have harmful effects on the environment and health, so it is preferable to treat them before they are discarded.

The choice of natural phosphate comes from the fact that phosphate ores are known for their ability to establish bonds with organic molecules of different sizes due to their physicochemical properties and diversity of chemical composition, its low cost and their use without any pre-treatment. In addition, this study examined the effects of different parameters such as adsorbent dose, dye solution pH, initial concentration, and temperature on the removal efficiency of MO and MB dyes by adsorption. The thermodynamics of adsorption were also evaluated.

2. METHODOLOGY

2.1 Samples and techniques

The phosphate used in this study was extracted from the Khouribga-Morocco region. It was used in crude form, and without prior purification; only particles of size between 180-125 µm were used. Particle size was measured using a set of vertically stacked sieves (Retsch) with mesh sizes between 90 and 500 µm. A mass of material was shaken and vibrated to pass through the sieves for 5 min and the retained quantity on each sieve was weighed. A phosphate portion was further calcined in a porcelain boat at 500°C in a tubular furnace. The interest of the calcination of phosphate sample was essentially the elimination of a part of the organic matter in gaseous form (CO_2) to study its effect on the adsorption, and the choice of this temperature, which is not high, was to preserve the basic amorphous morphology of this material. The obtained products were denoted as non-calcined NP and calcined NP, and then characterized using the following techniques:

X-ray fluorescence (XRF) was used to analysis the chemical composition of both samples. The elemental composition was determined by a Axios wavelength dispersive XRF spectrometer (Epsilon 3X, Manufacturer PANalytical, Netherlands). Samples were prepared in the form as compacted powder into pellets (PROT-ELE03-v01).

X-ray diffraction (XRD) measurements were recorded on a D2 Phaser powder diffractometer (Manufacturer Bruker, Germany) equipped with a copper anticathode (CuK_α line, λ=1.5406 Å) operating at 30 kV and 10 mA. The samples were irradiated in an angular range of 2θ of 10° to 80° with a 0.01° measurement pitch and a 0.5 sec/step count time.

Infrared spectroscopy measurements were obtained using a Perkin Elmer FTIR-2000 spectrophotometer (Netherlands). The results are presented in transmittance for wavenumbers between 4,000 and 400 cm^{-1}. The samples are packaged as pellets, consisting of 1 mg of the solid, diluted in 100 mg of KBr.

The specific surface area of non-calcined and calcined NP was determined from N_2 adsorption at -196°C using the BET method on a Quantasorb junior apparatus which provides only the specific surface. Samples were degassed for half an hour at 150°C before measurements.

2.2 Adsorption studies

The required initial dye concentrations were prepared by dissolving the desired weight of each dye in distilled water. The sorption processes were carried out in graded beakers containing the desired adsorbent dose and 200 mL of the colouring solution at a given concentration. These experiments were carried out with constant agitation and varying the pH of the solution, the phosphate solids dose 0-14 g/L, the contact time from 0 to 180 min and the starting dye concentration of 10 to 40 mg/L at five temperatures from 10 to 50°C which was controlled using a Cryothermostat. The pH was adjusted by adding sodium hydroxide or nitric acid solution. At the given time intervals, about 3 mL of the sample mixtures were collected and then filtered to separate the solid from solution using a syringe attached to a Sartorius filter (Porosity 0.2 µm). The maximum absorption wavelengths are 665 and 465 nm for methylene blue and methyl orange, respectively. The adsorption capacity was calculated using Equation 7 in Table 1.

Table 1. Mathematical equations and models using in this adsorption study

Eq. No.	Formula	Functionality	Parameters and/or assumptions	References
1	$\frac{dq}{dt} = k_1(q_e - q_t)$	Speed law equation: pseudo-first-order model	- q_t and q_e are the adsorbed quantity at time t and equilibrium respectively, in (mg/g), k_1 is the pseudo-first order velocity constant (min^{-1}), and t is the contact time (min). - Adsorption is considered reversible	Lagergren (1898)
2	$q = q_e(1 - e^{-k_1 t})$	Integration of speed law equation		
3	$\frac{dq}{dt} = k_2(q_e - q_t)^2$	Pseudo-second-order model	q_t and q_e in (mg/g), are the adsorbed quantity at time t and equilibrium respectively, k_2 (g/mg·min) is the rate constant of pseudo-second order adsorption and t is the contact time (min).	Ho and Mckay (1998)
4	$q_t = \frac{k_2 q_e^2 t}{1 + k_2 q_e t}$	Integration of differential equation		
5	$q_e = \frac{q_m K_L C_e}{1 + K_L C_e}$	Langmuir isotherm model	- K_L: direct measure of the intensity of the adsorption process; q_m: maximum adsorption capacity - Uniform energetic adsorption sites, single-ply coverage, and no lateral interaction between adsorbed molecules.	Langmuir (1916) Pignatello (1999)
6	$q_e = K_f C_e^{1/n}$	Freundlich isotherm model	K_F: adsorption maximum capacity; n: adsorption behavior; q_e: amount adsorbed per gram of solid, C_e: concentration of adsorbent at adsorption equilibrium	Freundlich and Heller (1939); Tóth (1994)
7	$q = \frac{(C_0 - C)}{R}$	Adsorption capacity	q is the adsorbed quantity (mg/g), C_0 (mg/L) is the initial dye concentration, C (mg/L) is the dye concentration at t and R (g/L) is the mass adsorbents per liter of solution.	Assimeddine et al. (2020)
8	$R_L = \frac{1}{1 + K_L C_0}$	Adsorption feasibility	C_0 is the initial concentration of the dye (mg/L), and K_L is the Langmuir constant (L/mg).	Yous et al. (2018)
9	$\Delta G^\circ = -RT\ln(K_D)$	Gibbs free energy	- $\Delta G°$: Gibbs free energy change; K_D: an equilibrium distribution constant (dimensionless) $K_D = \frac{q_e}{C_e}$; R the universal gas constant (8,314 J/mol K), and T is the solution's temperature (K). - $\Delta S°$: entropy variation; $\Delta H°$: enthalpy variation	Machrouhi et al. (2020)
10	$\ln K_D = -\frac{\Delta H^\circ}{RT} + \frac{\Delta S^\circ}{R}$	Van't Hoff		

2.3 Adsorption kinetics and isotherms models

Diverse theoretical adsorption kinetic (pseudo-first-order and pseudo-second-order) and Freundlich and Langmuir isotherm models are applied to experimental data in order to determine the best-fitting model as shown in Table 1. The Langmuir model considers that the adsorption sites are uniformly energetic, that they are covered by a single layer and that there is no lateral interaction between the adsorbed molecules. Graphically, a saturation point is reached at equilibrium (Langmuir, 1916). The Freundlich isotherm model considers that the number of sites likely to adsorb the compound is unlimited. Thus, the Freundlich isotherm has no maximum unlike that of Langmuir. This empirical model is widely used for the practical representation of adsorption equilibrium (Freundlich and Heller, 1939).

3. RESULTS AND DISCUSSION

3.1 Characterization

3.1.1 X-ray fluorescence

X-ray fluorescence chemical analysis is a non-destructive technique used to quantify the elemental composition of a sample. The percentages by mass of the oxides found in the uncalcined and calcined at 500°C natural phosphates are presented in Table 2.

It can be seen that the lower levels of P_2O_5 and higher amounts of CaO indicate the presence of other mineral phrases containing calcium such as calcite ($CaCO_3$) and gypsum ($CaO+SO_3$) in addition to apatite. Indeed, the percentage ratio of CaO/P_2O_5 obtained by XRF (equal to 3.04 for non-calcined NP and 3.18 for calcined NP) is greater than that calculated from fluorapatite (equal to 1.31). There is also silica (SiO_2) and lower contents of Al_2O_3, Fe_2O_3, MgO, and SO_3. The increase in the percentages of oxides that form phosphate after calcination at 500°C is due to the calcination eliminating part of the organic matter in gaseous form (CO_2) and water (Mgaidi et al., 2004), subsequently increasing the contents of the remaining elements. It should also be noted that other metals (Pb, Cu, Cd, Cr, Zn, Ti,…) were detected in the ppm range.

3.1.2 X-ray diffraction

X-ray diffraction analysis of non-calcined and calcined natural phosphates at 500°C, as shown in Figure 1, shows that these materials are well crystallized and they are mainly composed of a fluorapatite carbonated mineral (also known as francolite), which is derived from an ore fluorapatite $Ca_{10}(PO_4)_6F_2$ (Kenzour et al., 2019; Gallala et al., 2016; Fahami and Nasiri-Tabrizi, 2014). Carbonate-fluorapatite have an essential substitution in the crystal lattice of carbonate apatite, Ca^{2+} cations by Na^+, K^+, Mg^{2+}..., and also by the partial substitution of phosphate and/or fluoride ions by carbonate ions, which leads to the formation of B- and/or A-type carbonate-fluorapatite (Madupalli et al., 2017; Fleet and Liu, 2008), respectively. Phosphate ores also contain secondary minerals, or gangue impurities including contents of quartz (SiO_2), calcite ($CaCO_3$), and carbonates, which are in the form of dolomite $CaMg(CO_3)_2$ (Kenzour et al., 2019). XRD also reveals the presence of weak amounts of fluorapatite evident by the 2θ=11° peak. The diffractograms show that with calcination at 500°C, the diffraction lines become more resolute and intense (2θ=20.8°, 23.0°, 26.6°, 29.4°, 39.3°, 47.5°, 57.5°); which reflects an improvement in the crystalline quality of the phosphate studied. On the other hand, there was a decrease in the intensity of the lines corresponding to carbonate-fluorapatite due to calcination, which acts on the elimination of some carbonates.

Table 2. Mineralogical composition of natural phosphate (non-calcined and calcined).

Compounds	wt% of non-calcined NP	wt% of NP calcined at 500°C
CaO	34.337	49.086
P_2O_5	11.281	15.407
SiO_2	1.479	6.959
Al_2O_3	0.584	2.007
Fe_2O_3	0.262	0.693
MgO	0.231	0.692
SO_3	0.541	0.630
K_2O	**	0.177
TiO_2	**	0.161
Cr_2O_3	**	0.105

3.1.3 Infrared spectroscopy

To determine the carbonates type of the fluorapatite indexed by the XRD analysis, we recorded the IR absorbance spectra of the phosphate solids. Figure 2 corresponds to the infrared absorption spectra of non-calcined and calcined natural phosphates at 500°C. The strong band observed around 1,040 cm^{-1} is attributed to asymmetric stretching vibration ν_3 of PO_4 phosphate anions, which broadened by shoulder band at 1,080 cm^{-1} can be assigned also to ν_3 PO_4^{3-} (Furuzono et al., 2001). The bands centered at 576 cm^{-1} (it becomes shoulder after

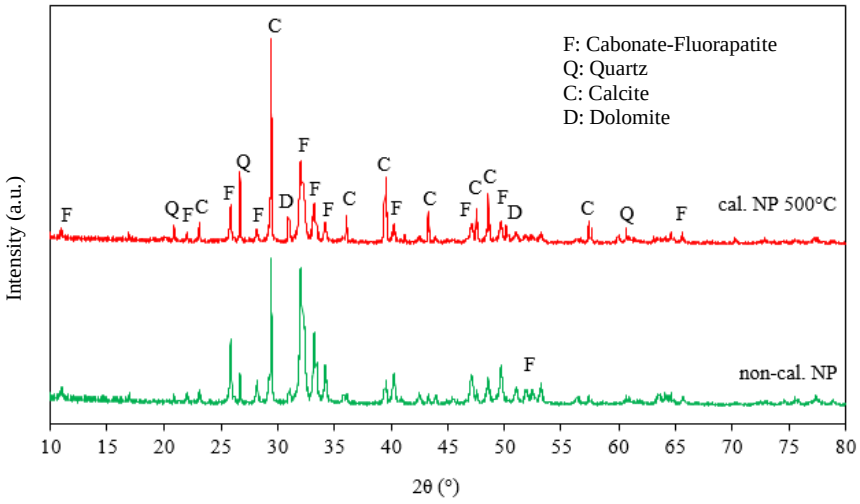

Figure 1. XRD patterns of the non-calcined and calcined natural phosphate

calcination) and 606 cm^{-1} can be assigned to out-of-plane bending vibration ν_4 of phosphate group (PO_4^{3-}) (Dakkach et al., 2012; Sadiq et al., 2015). The band located at 480 cm^{-1} is attributed to the symmetrical strain mode ν_2 (PO_4^{3-}) (Drouet, 2013). The spectra of solids exhibit the shoulder for orthophosphates (PO_4^{3-}) ions, at 966 cm^{-1}. It is attributed to symmetric stretching vibration ν_1 of phosphate PO_4^{3-} (Drouet, 2013). The doublet located around 1,428 and 1,454 cm^{-1}, is associated to ν_3 (CO_3^{2-}), while the absorption band observed at 872 cm^{-1} is assigned to the ν_2 bending vibrations of the carbonate group (CO_3^{2-}) (Zahrani and Fathi, 2009; Nikcevic et al., 2004), consistent with the carbonate fluorapatite spectra previously reported by Fleet (2009) and Wang et al. (2018). It corresponds to the out-of-plane oscillating motion of C atoms. The wavenumbers of carbonate vibrations illustrated in Figure 2 show the characteristic bands of type B carbonate- fluorapatite (CO_3^{2-} substitute PO_4^{3-} ions). Therefore, the intensities of all bands corresponding to CO_3 and PO_4 vibrational modes in the calcined phosphate were lower relative to non-calcined phosphate, possibly indicating the transfer of a carbonate amount from carbonated-fluorapatite into calcite and dolomite (Figure 2). This confirms the results obtained by XRD (Figure 1).

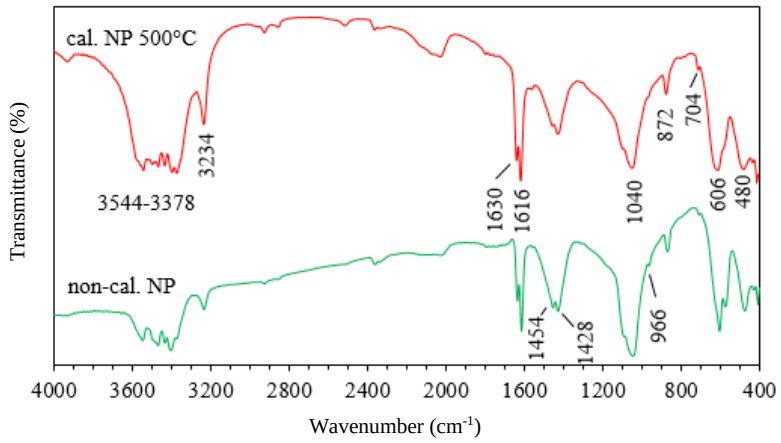

Figure 2. FT-IR spectra of non-calcined and calcined natural phosphate

Both bands at 1,616 and 1,630 cm^{-1} are due to the bending vibration of the hydroxyl (OH^-) (H-O-H) (Nikcevic et al., 2004; Yous et al., 2018; Aines and Rossman, 1984; Boughzala and Bouzouita, 2015). A series of vibrations was observed in the 3,200-3,550 cm^{-1} region which could be assigned to OH group vibrations bound by hydrogen bonds (O-H asymmetrical and symmetrical stretching vibrations). The additional shoulder at 704 cm^{-1} can be assigned to free vibration of OH (ν_L(O-H) (Nikcevic et al., 2004; Wang et al., 2018). No band was observed at 880 cm^{-1}, which is assigned to the A-type carbonate and

can be found in the spectra of natural phosphate, as reported previously by Madupalli et al. (2017).

3.1.4 Specific surface area

The specific surface area of non-calcined and calcined NP was 27 and 32 m^2/g, respectively. These BET surface area values remained low compared to other adsorbents such as activated carbon (Wang et al., 2017). A slight increase after calcination of sample may be due to the creation of new sites by the release of volatile molecules.

3.1.5 pH zero charge point (pH_{pzc})

The pHpzc (zero charge point pH) is the pH value at which the net adsorbent surface charge is zero. This is a key parameter in adsorption processes, especially when electrostatic forces are implied in the mechanisms. The pHpzc is determined by the pH drift method, which consists in adjusting the pH of NaCl solutions with a concentration of 0.01 M and a volume of 50 mL (pH values between 2 and 12) by adding a solution of NaOH or HCl (0.1 M). Then, a mass of 0.05 g of the phosphate sample added to each volume. The suspensions must be kept stirring at room temperature for 6 h, and the final pH is then measured. Furthermore, the natural phosphate used is insoluble in water at different pH studied (acidic and basic).

We have plotted the evolution of the final pH as a function of the adjusted initial pH (Figure 3). The point of intersection between the curve obtained and that of the bisector corresponds to the pHpzc, which equals 8. As well as for pH higher than pHpzc, the adsorbent surface would be negatively charged so that the cations can be adsorbed, while for pH lower than pHpzc, the surface would be positively charged so that the anions can be adsorbed.

3.2 Adsorption studies

3.2.1 Adsorbent dose

Figure 4 shows the percentage of removal of methyl orange (MO) and methylene blue (MB) dyes as a function of the crude phosphate dose, with a contact time of 3 h. It can be seen that the degree of discoloration rises as the mass of natural phosphate adsorbent increases. For MB, the total staining of solution is extinguished at around 1 g/L, while for MO, the solution remains colored even at 14 g/L, the percentage of elimination stabilizes almost at 20% for a mass ratio of 10 g/L. This is can be explained by the anionic (MO) and cationic (MB) nature of adsorbate and surface charge of adsorbent without any modification of solution initial pH (pH_i=9).

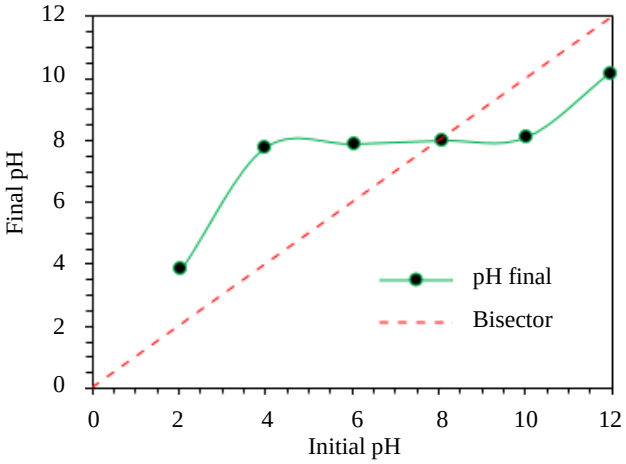

Figure 3. pH zero charge point of natural phosphate (NP)

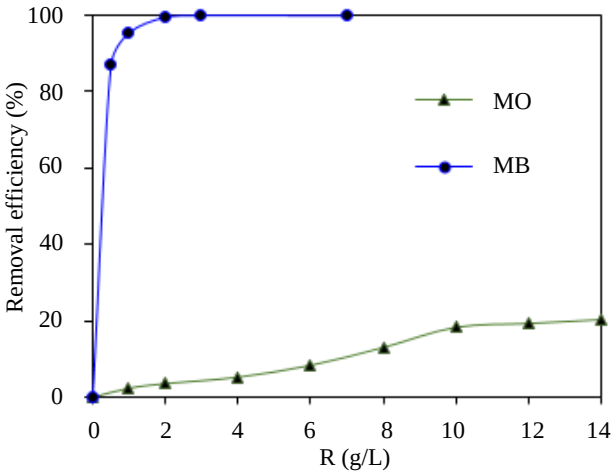

Figure 4. Effect of adsorbent dose on MB (C_0=10 mg/L) and MO (C_0=20 mg/L) adsorption

3.2.2 Removal efficiency by non-calcined and calcined phosphate

Figure 5 shows the comparison of dye removal efficiency of the solutions prepared by adsorption on uncalcined and calcined phosphate at 500°C. The curves show that the adsorption mechanism is almost the same for both MB and MO dyes. This can be explained by the fact that both samples have similar structural properties and compositions, according to the results obtained from their characterization. It can be concluded that a calcination temperature of 500°C does not result in a significant difference in the texture of the phosphate studied. So, in the rest of the work, we limited ourselves to the examination of the adsorption capacity of the non-calcined crude phosphate.

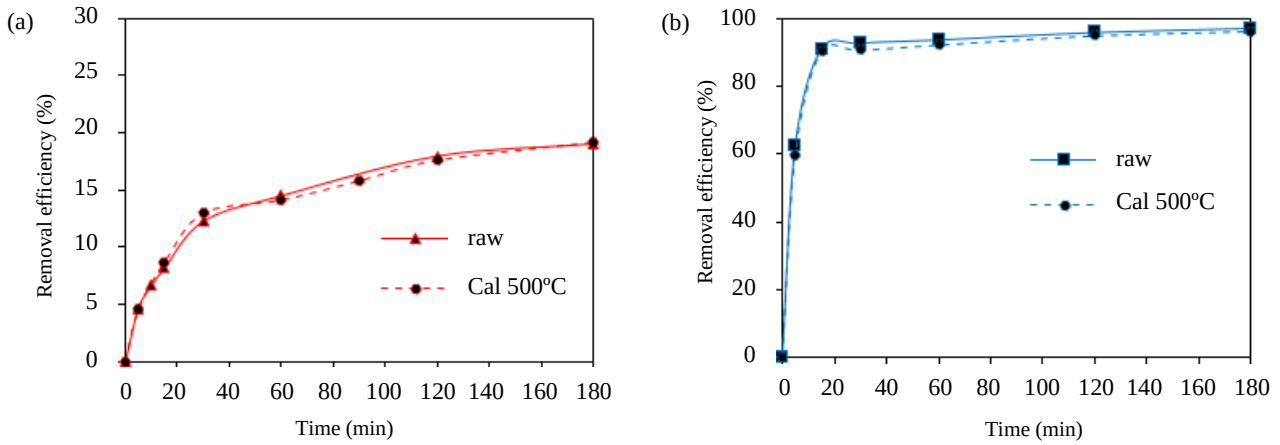

Figure 5. Adsorption kinetics by non-calcined and calcined phosphate at pHi=9 of MO (a): C_0=20 mg/L, R=10 g/L; and of MB (b): C_0=10 mg/L, R=1 g/L

3.2.3 Effect of pH on dyes removal

The pH is a more important parameter in the adsorption process, as it can influence both the adsorbent surface and adsorbate structure as well as the mechanism of adsorption (Elmoubarki et al., 2017). For this, we carried out several adsorption tests in different pH values. The experimental results presented in Figure 6 clearly show that the pH has a strong influence on the adsorption of the anionic dye MO, in which the percentage of discoloration is canceled out in the most basic pH, while the elimination is more favorable in the acidic medias, it reaches 60% for a pH value of 4. For MB, the rate of elimination increases with increasing pH value. It went from 75% for a more acidic pH (pH=2) and arrived at 99% for a basic pH equal 12. These results can be explained that when the pH of the solution is lower (pH<pHpzc), the richer the solution is in hydrogen ions. The number of positively charged sites increases and the surface of the phosphate solid become positively charged, and therefore likely to attract the negative charges of the anionic dye (MO) (Guo et al., 2013). On the other hand, at pH superior to pHpzc, the surface is negatively charged, which promotes adsorption of the cationic dye. The initial adsorption of dyes was higher compared to the equilibrium point, due to the high activity (strength and numbers) of the initial sites available on the material surface. Equilibrium was reached at 30 min and 60 min for BM and MO, respectively, followed by plateaus signifying equilibrium, and this is valid for all pH values. In the sequel of this work, we kept the pH of the solution for the MO dye at 4, by adjustment with nitric acid solution, because the pH of the colored solution reached a value of 9, once the NP is added, and we have found that the adsorption of MO almost canceled out at basic pH.

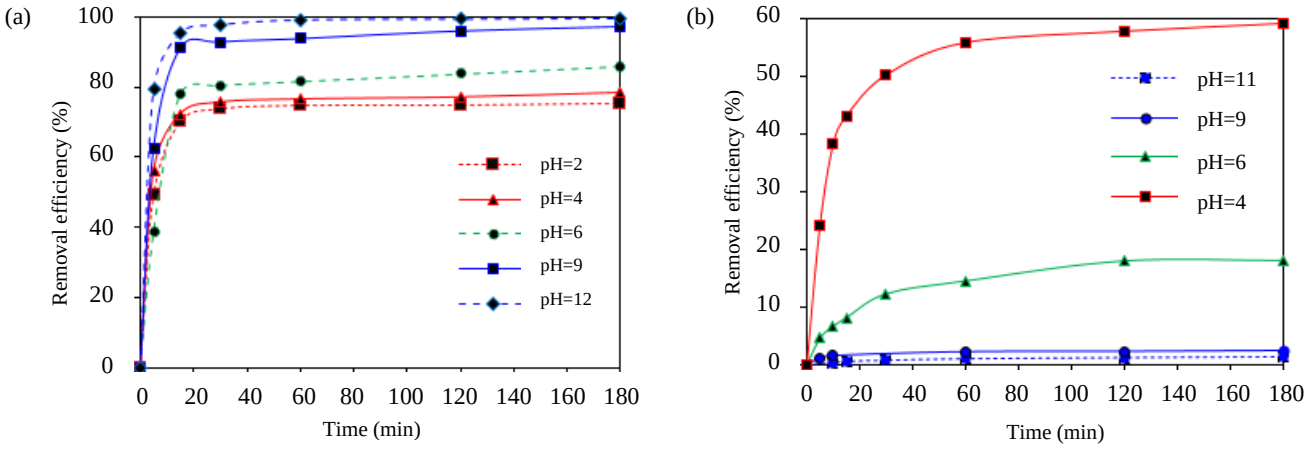

Figure 6. pH effect on adsorption of MB (a): C_0=10 mg/L, R=1 g/L and of MO (b): C_0=20 mg/L, R=10 g/L

3.2.4 Effect of initial dye concentration

The initial dye concentration affects its kinetics and the adsorption capacity; for this, the initial concentration of dye was varied from 10 to 50 mg/L. The results obtained are presented in Figure 7, which show that the adsorption process starts with a short transient regime and ends with a steady state. The curves show that the adsorbed quantity rises rapidly during the first 30 min for MB and 60 min for MO until reaching a plateau whatever the concentration. This may be due to the saturation of all active sites on the surface of the phosphate material. The adsorbed amount increases from 3.2 to 10.2 mg/g in the case of MB and from 0.3 to 2.8 mg/g in the case of MO for concentrations ranging from 10 to 50 mg/L. According to the curves, the concentration threshold has not been reached since the plateaus are far from each other and are approaching each other for MB at higher concentrations. Increasing the initial concentration enhances the interaction between the adsorbate molecules and the adsorbent particles, thus increasing the adsorption capacity. More, increasing the initial dye concentration induces an increase in the driving force of the concentration gradient, hence increasing the diffusion of the dye molecules in solution through the adsorbent surface (Deniz and Saygideger, 2010). A similar trend has been described for the adsorption of methyl orange dye onto mesoporous carbon by Mohammadi et al. (2011) and methylene blue onto activated carbon by Kuang et al. (2020).

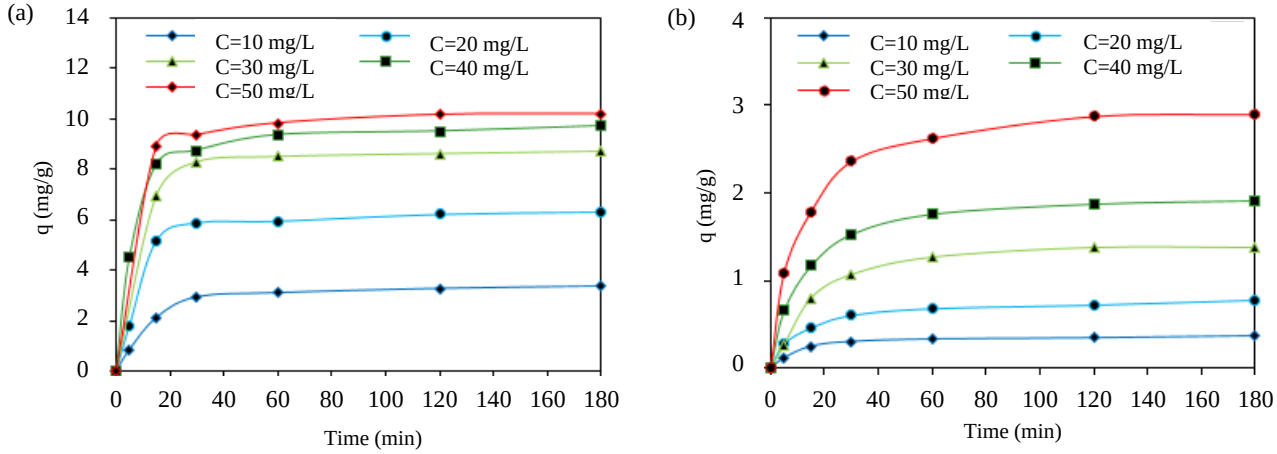

Figure 7. Effect of initial concentration: MB (a): dye at R=1 g/L, pH=9 and MO (b): dye at R=10 g/L, pH=6

3.2.5 Adsorption isotherms

The adsorbed quantities at equilibrium (qe), as a function of the equilibrium concentration of each dye, are shown in Figure 8. The experimental results obtained were compared with adsorption isotherm models of Langmuir (Langmuir, 1918) and Freundlich (1906). All constants involved in the expression of each model were calculated by non-linear regression analysis and presented in Table 3. From Figure 8 we can notice that the adsorption of dyes at equilibrium increases with increasing concentration at equilibrium, this was due to a high driving force for the mass transfer of the dye at high concentration in solution.

Table 3. Constants for isothermal models of dyes adsorption on natural phosphate

Dyes	q_m (mg/g)	Langmuir		K_F ($mg^{1-1/n}/L^{1/n}/g$)	Freundlich	
		K_L (L/mg)	r^2		n	r^2
MB	10.3321	1.7811	0.98921	5.93569	4.92987	0.89382
MO	25.9014	0.0050	0.84625	0.02011	0.60961	0.99554

It can be seen from the values of the correlation coefficients r^2, the Langmuir model best describes the adsorption isotherm of MB. This result indicates that the adsorption process takes place in a monolayer, where all adsorption sites on adsorbent surface are energetically uniform, and there are no lateral interactions between the adsorbed molecules. It can be seen graphically that a saturation point is reached where no further adsorption can occur afterwards, this is a plateau which characterizes the Langmuir

isotherm at equilibrium. The constant called the separation factor whose Langmuir isotherm characteristic can be expressed in the form established by Equation 8 in Table 1.

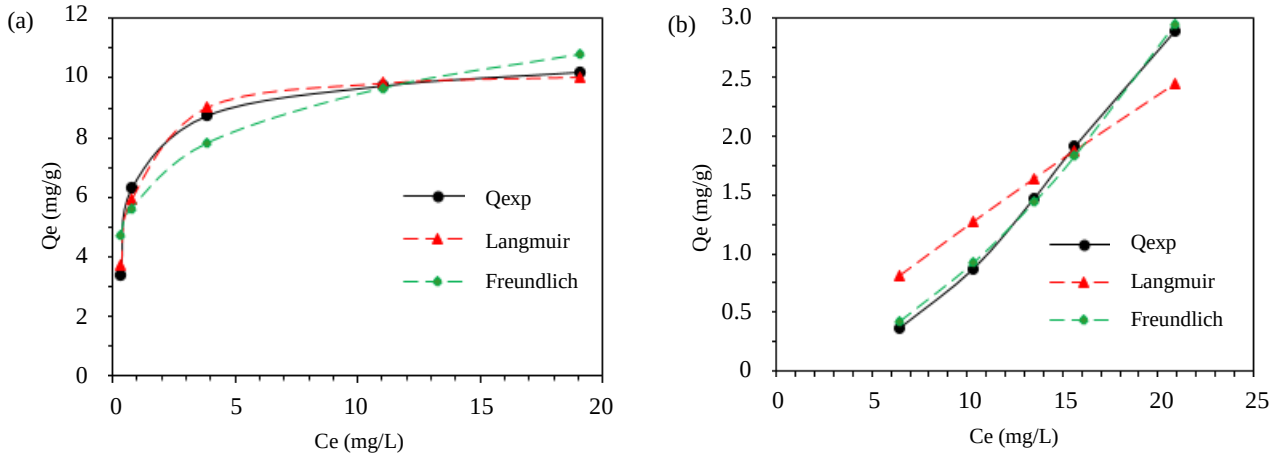

Figure 8. Adsorption isotherms for MB (a): dye at R=1 g/L, pH=9 and MO (b): dye at R=10 g/L, pH=6

Three cases of adsorption can be distinguished according to the value of R_L, the adsorption is unfavorable when the separation factor value is strictly superior to one, if the R_L=1 the adsorption is said to be linear, when $0<R_L<1$ the adsorption is said to be favorable (Yous et al., 2018). The measured values for the studied dyes are less than one and more than 0 (R_L=0.053 for MB and 0.909 for MO). This reveals favorable adsorption of MB and MO over adsorbent surface.

Linearity also shows that the adsorption isotherm of MO follows the Freundlich model, based on the heterogeneous sorption surface where the number of sites that can adsorb the compound is unlimited. Thus, this isotherm does not present a maximum. The shape of the isotherm will depend on the value of 1/n, which represents the absorption intensity; in this case, we have 1/n>1, representing the S-type convex isotherm according to Giles classification (Giles et al., 1960), in which the adsorbate- adsorbent interactions take place due to electrostatic attractions, but also adsorbate-adsorbate, due to intermolecular interactions.

3.2.6 Adsorption kinetics

The two kinetic models, pseudo-first order and pseudo-second order, have been examined to characterize the kinetics involved in the adsorption process of both MB and MO dyes. The kinetic data were evaluated by the values of the correlation coefficient (r^2) and the quantity adsorbed at equilibrium of dye. The parameters were estimated using non-linear regression.

The kinetics results of the adsorption of methylene blue and methyl orange by non-calcined NP are presented in Table 4 and Figure 9. The figure indicates that the removal of cationic MB and anionic MO were very rapid in the first 30 min of contact time; the adsorption capacity of the dyes reached 0.91 mg/g and 8.35 mg/g for MO and MB, respectively. After this period, the rate of removal was slower and stagnated with the increase in contact time. Around 90% of the quantity of dye adsorbed at the end of equilibrium was carried out in the period 0-30 min. At 180 min, adsorption capacity stabilizes at 1.09 mg/g for the MO and 9.54 mg/g for the MB dyes.

According to the results obtained, the two models give a reasonably good fit to the experimental data, but the pseudo-second order model is found to be the most suitable to describe the adsorption dynamics of the two dyes on the phosphate due to the excellent correlation of the parameters calculated by the model with the experimental data. Our results are in accordance with that reported by others works (Assimeddine et al., 2020; Elmoubarki et al., 2015; Mahjoubi et al., 2016). They showed that the adsorption process of the same dyes on clays and layered double hydroxides (LDH) absorbents obeys the pseudo-second-order model. This model allows the characterization of adsorption kinetics by taking into account both the rapid uptake of solutes at the most reactive sites and the slow uptake at low energy sites.

Table 4. Kinetic parameters of adsorption of MB and MO on natural phosphate

Dyes	Pseudo-first-order				Pseudo-second-order		
	qe (exp) (mg/g)	qe (mg/g)	k_1 (L/min)	r^2	qe (mg/g)	k_2 (g/mg·min)	r^2
MB	9.540906	9.15594	0.08868	0.9836	10.00316	0.01308	0.99472
MO	1.091152	1.04556	0.09365	0.99073	1.140725	0.11214	0.99579

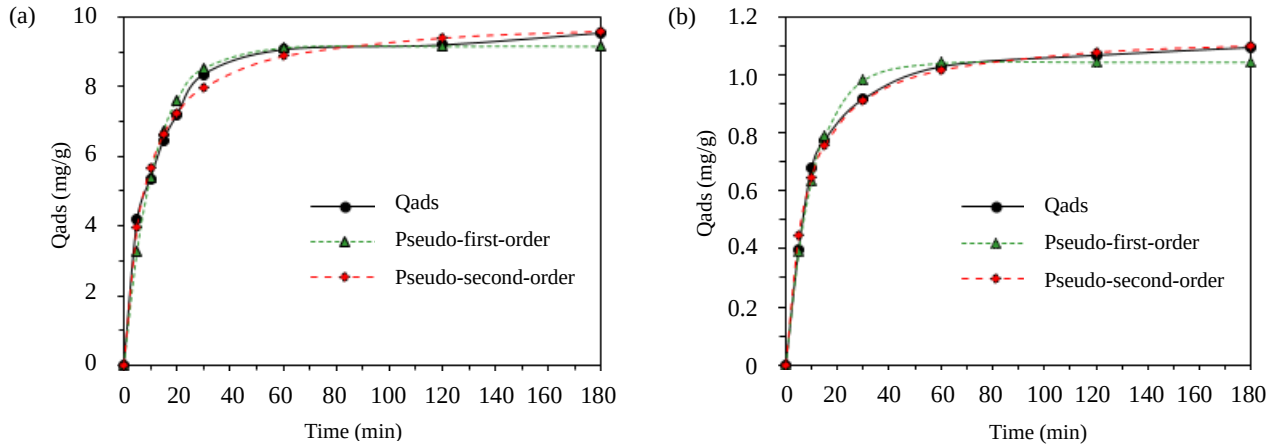

Figure 9. Adsorption kinetics, pseudo-first-order and pseudo-second-order of MB (a) and MO (b)

3.2.7 Effect of temperature and thermodynamic study

Depending on the type of adsorbent material and the nature of the adsorbed molecules, adsorption is a process that can be endothermic or exothermic (Rytwo and Ruiz-Hitzky, 2003). To make a thermodynamic study of the phenomenon of adsorption of dyes such as methylene blue and methyl orange by crude phosphate, we carried out discoloration tests by varying the temperature of colored solutions from 10 to 50°C, because the effect of temperature on the dye adsorption is very important in the adsorption mechanism. Figure 10 represents the percent removal of BM and OM on crude phosphate as a function of solution temperature. The curves in the figure indicate that increasing the solution temperature leads to an increase in removal efficiency (%), which promotes MB adsorption, suggesting an endothermic process. This probably results from an increase in the number of active adsorption sites, via the release of new sites, with increasing temperature. Moreover, an increase in temperature promotes the diffusion of molecules through the outer boundary layer to the inner pores of the adsorbent particles, this may be due to the decrease in the viscosity of the solution and the increase in the concentration of monomers in the solution. These results are in agreement with those found by Al-Ghouti et al. (2005) on a study of MB adsorption by manganese-oxides-modified diatomite. In contrast, other studies show that temperature change has almost no or little influence on the efficiency of MB adsorption by raw maize corncob (Farnane et al., 2018) or by clays (Elmoubarki et al., 2015), respectively. Thus, it is noticed that the effect of temperature could be related to the nature of the adsorbent particles. On the other hand, the removal of MO decreases significantly with increasing temperature, is due to the presence of desorption steps in the adsorption mechanism, in agreement with Arrhenius'law, suggesting that the surface reaction is exothermic.

From the results obtained, we determined the thermodynamic parameters of adsorption such as enthalpy (ΔH°) and entropy (ΔS°), which were estimated respectively from the slope and intercept of the ln(K_D) vs. 1/T plot, and free energy (ΔG°), using the Equations 9 and 10 in Table 1. From the calculated constants which are shown in Table 5, we can confirm that the adsorption process is endothermic for MB (positive ΔH°), then, the negative values of ΔG° are accompanied by a decrease with the rise in temperature indicates that the adsorption is spontaneous and more feasible at higher temperatures (Machrouhi et al., 2020). The value of the standard enthalpy, higher than 40 kJ/mol, can tell us that adsorption is chemical nature. In the case of MO,

according to the value of ΔH° the adsorption is exothermic, and this is physisorption type. It is also noted that ΔG° increases with increasing temperature, indicating a decrease in adsorption feasibility of MO dye onto phosphate materials.

Furthermore, it can be seen from the values of ΔS° that the randomness increases for MB (ΔS°>0) and decreases for MO (ΔS°<0) at the solid/ solution interface in the course of the dyes adsorption onto the surface of natural phosphate.

Table 5. Thermodynamic parameters calculated for adsorption

T (°C)	BM				OM			
	K_D	ΔG° (kJ/mol)	ΔH° (kJ/mol)	ΔS° (J/K mol)	K_D	ΔG° (kJ/mol)	ΔH° (kJ/mol)	ΔS° (J/K mol)
10	6.818	-4.519			0.134	4.734		
20	12.301	-6.117			0.107	5.435		
30	29.472	-8.528	56.421	214.43	0.090	6.066	-16.042	-73.181
40	64.714	-10.857			0.076	6.695		
50	121.666	-12.899			0.055	7.782		

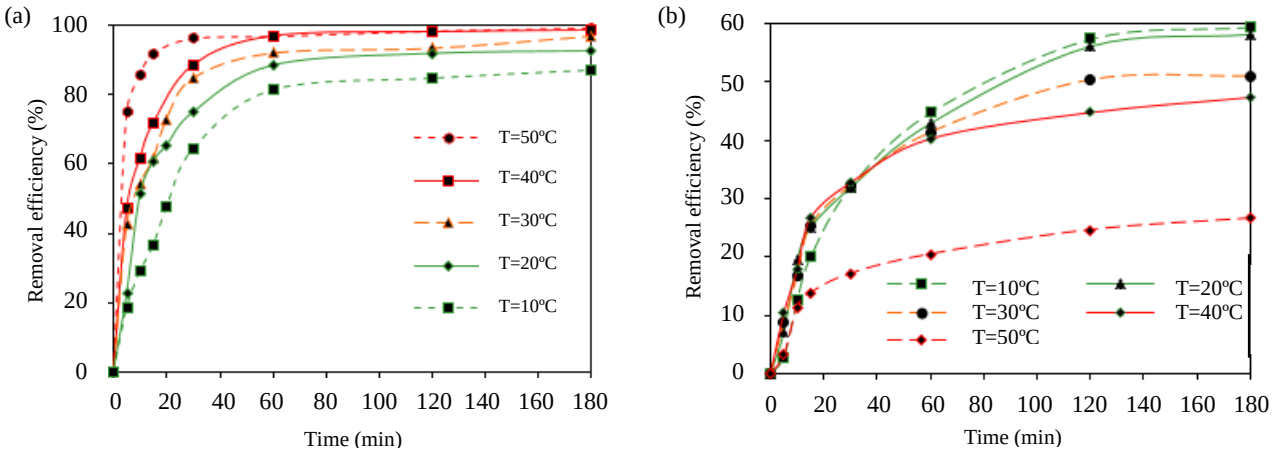

Figure 10. Effect of temperature on adsorption over crude phosphate of MB (a): R=1 g/L, pH=9 and MO (b): R=10 g/L, pH=6

4. CONCLUSION

This modest work examined the potential of a local natural phosphate, from the Khouribga-Morocco region, in the removal of cationic and anionic dyes from an aqueous solution. Different adsorption parameters such as contact time, initial dye concentration, adsorbent dose, pH of the initial solution and temperature were optimized. Experimental results of the adsorption tests showed that the phosphate material follows a pseudo-second-order adsorption kinetics for MO and MB dyes. This material exhibited high adsorption capacity at a more basic pH for the cationic dye MB (9.54 mg/g) and at a more acidic pH for the anionic dye MO (1.09 mg/g). The adsorption capacity of natural phosphate increases with the increase in the initial concentration of dyes, and the complete saturation of all surfactant sites on the material is reached at 30 min for MB and 60 min for MO, then the appearance of an equilibrium plateau. Increasing the temperature of the solution increases the removal efficiency (%) of methylene blue and decreases that of methyl orange. The adsorption process is spontaneous (ΔG° negative) and endothermic (ΔH° positive) for MB and exothermic for MO. Finally, the present study has shown that the local natural phosphate appears to be a good adsorbent candidate for the decoloration of dye-containing effluents.

ACKNOWLEDGEMENTS

The authors thank all who assisted in conducting this work.

REFERENCES

Al-Ghouti M, Khraisheh MAM, Ahmad MNM, Allen S. Thermodynamic behaviour and the effect of temperature on the removal of dyes from aqueous solution using modified diatomite: A kinetic study. Journal of Colloid and Interface Science 2005;287:6-13.

Aines RD, Rossman GR. Water in minerals? A peak in the infrared. Journal of Geophysical Research: Solid Earth 1984;89:4059-71.

Assimeddine M, Abdennouri M, Barka N, Rifi EH, Sadiq M. Physicochemical characterization of Moroccan natural clays and the study of their adsorption capacity for the methyl orange and methylene blue removal from aqueous solution. Journal of Environmental Treatment Techniques 2020; 8(4):1258-67.

Barka N, Assabbane A, Nounah A, Laanab L, Aît- Ichou Y. Removal of textile dyes from aqueous solutions by natural phosphate as a new adsorbent. Desalination 2009;235:264-75.

Bedin KC, de Azevedo SP, Leandro PKT, Cazetta AL, Almeida VC. Bone char prepared by CO_2 atmosphere: Preparation optimization and adsorption studies of Remazol Brilliant Blue R. Journal of Cleaner Production 2017;161:288-98.

Bensalah H, Bekheet MF, Younssi SA, Ouammou M, Gurlo A. Removal of cationic and anionic textile dyes with Moroccan natural phosphate. Journal of Environmental Chemical Engineering 2017;5(3):2189-99.

Boughzala K, Bouzouita K. Synthesis and characterization of strontium-calcium-lanthanum apatites $Sr_{7-x}Ca_xLa_3(PO_4)_3(SiO_4)_3F_2$ $0\leq x\leq 2$. Comptes Rendus Chimie 2015;18(8):858-66.

Chen BY. Toxicity assessment of aromatic amines to *Pseudomonas luteola*: Chemostat pulse technique and dose-response analysis. Process Biochemistry 2006;41(7):1529-38.

Combes RD, Haveland-Smith RB. A review of the genotoxicity of food, drug and cosmetic colors and other azo, triphenylmethane and xanthene dyes. Mutation Research/Reviews in Genetic Toxicology 1982;98(2):101-248.

Dakkach M, Atlamsani A, Sebti S. Natural phosphate modified by vanadium: A new catalyst for oxidation of cycloalkanones and α- ketols with oxygen molecular. Comptes Rendus Chimie 2012;15(6):482-92.

Damodar RA, Jagannathan K, Swaminathan T. Decolourization of reactive dyes by thin film immobilized surface photoreactor using solar irradiation. Solar Energy 2007;81(1):1-7.

Daneshvar N, Salari D, Khataee AR. Photocatalytic degradation of azo dye acid red 14 in water: Investigation of the effect of operational parameters. Journal of Photochemistry and Photobiology A: Chemistry 2003;157(1):111-6.

Deniz F, Saygideger SD. Investigation of adsorption characteristics of Basic Red 46 onto gypsum: Equilibrium, kinetic and thermodynamic studies. Desalination 2010;262 (1-3):161-5.

Drouet C. Apatite formation: Why it may not work as planned, and how to conclusively identify apatite compounds. BioMed Research International 2013;2013(4):1-12.

Elmoubarki R, Mahjoubi FZ, Elhalil A, Tounsadi H, Abdennouri M, Sadiq M, et al. Ni/Fe and Mg/Fe layered double hydroxides and their calcined derivatives: Preparation, characterization and application on textile dyes removal. Journal of Materials Research and Technology 2017;6(3):271-83.

Elmoubarki R, Mahjoubi FZ, Tounsadi H, Moustadraf J, Abdennouri M, Zouhri A, et al. Adsorption of textile dyes on raw and decanted Moroccan clays: Kinetics, equilibrium and thermodynamics. Water Resources and Industry 2015;9:16-29.

Fahami A, Nasiri-Tabrizi B. Mechanochemical behavior of $CaCO_3$-P_2O_5-CaF_2 system to produce carbonated fluorapatite nanopowder. Ceramics International 2014;40(9):14939-46.

Farnane M, Tounsadi H, Machrouhi A, Elhalil E, Mahjoubi FZ, Sadiq M, et al. Dye removal from aqueous solution by raw maize corncob and H_3PO_4 activated maize corncob. Journal of Water Reuse and Desalination 2018;8(2):214-24.

Fleet ME. Infrared spectra of carbonate apatites: ν_2-region bands. Biomaterials 2009;30(8):1473-81.

Fleet ME, Liu X. Accommodation of the carbonate ion in fluorapatite synthesized at high pressure. American Mineralogist 2008;93:1460-9.

Freundlich H, Heller W. The adsorption of cis- and trans-azobenzene. Journal of the American Chemical Society 1939;61:2228-30.

Freundlich HMF. Over the adsorption in solution. The Journal of Physical Chemistry 1906;57:385-471.

Furuzono T, Walsh D, Sato K, Sonoda K, Tanaka J. Effect of reaction temperature on the morphology and size of hydroxyapatite nanoparticles in an emulsion system. Journal of Materials Science Letters 2001;20(2):111-4.

Gallala W, Herchi F, Ben Ali I, Abbassi L, Gaied ME, Montacer M. Beneficiation of phosphate solid coarse waste from redayef (Gafsa Mining Basin) by grinding and flotation techniques. Procedia Engineering 2016;138:85-94.

Giles CH, MacEwan TH, Nakhwa SN, Smith D. Studies in adsorption**.** Part XI. A system of classification of solution adsorption isotherms, and its use in diagnosis of adsorption mechanisms and in measurement of specific surface areas of solids. Journal of the Chemical Society 1960;846:3973-93.

Guo Y, Zhu Z, Qiu Y, Zhao J. Enhanced adsorption of acid brown 14 dye on calcined Mg/Fe layered double hydroxide with memory effect. Chemical Engineering Journal 2013;219:69-77.

Gupta K, Khatri OP. Fast and efficient adsorptive removal of organic dyes and active pharmaceutical ingredient by microporous carbon: Effect of molecular size and charge. Chemical Engineering Journal 2019;378:Article No.122218.

Heiss GS, Gowan B, Dabbs ER. Cloning of DNA from a *Rhodococcus* strain conferring the ability to decolorize sulfonated azo dyes. FEMS Microbiology Letters 1992; 99:221-6.

Ho YS, Mckay FG. Kinetic models for the sorption of dye from aqueous solution by wood. Process Safety and Environmental Protection 1998;76:183-91.

Kenzour A, Belhouchet H, Kolli M, Djouallah S, Kherifi D, Ramesh S. Sintering behavior of anorthite- based composite ceramics produced from natural phosphate and kaolin. Ceramics International 2019;45:20258-65.

Kuang Y, Zhang X, Zhou S. Adsorption of methylene blue in water onto activated carbon by surfactant modification. Water 2020;12(2):587-605.

Lagergren S. About the theory of so-called adsorption of soluble substance. Kungliga Svenska Ventenskapsakademiens Handlingar 1898;24:1-39.

Langmuir I. The constitution and fundamental properties of solids and liquids. Part I. Solids. Journal of the American Chemical Society 1916;38:2221-95.

Langmuir I. The adsorption of gases on plane surfaces of glass, mica and platinum. Journal of the American Chemical Society 1918;40:1361-403.

Machrouhi A, Boumya W, Khnifira M, Sadiq M, Abdennouri M, Elhalil A, et al. Synthetic dyes adsorption and discoloration of a textile wastewater effluent by H_3PO_4 and H_3BO_3 activated *Thapsia transtagana* biomass. Desalination and Water Treatment 2020;202:435-49.

Madupalli H, Pavan B, Tecklenburg MMJ. Carbonate substitution in the mineral component of bone: Discriminating the

structural changes, simultaneously imposed by carbonate in A and B sites of apatite. Journal of Solid-State Chemistry 2017;255:27-35.

Mahjoubi FZ, Khalidi A, Abdennouri M, Barka N. M-Al-SO_4 layered double hydroxides (M=Zn, Mg, or Ni): Synthesis, characterization and textile dyes removal efficiency. Desalination and Water Treatment 2016;57:21564-76.

Mgaidi A, Ben Brahim F, Oulahna D, Nzihou A, El Maaoui M. Chemical and structural changes of raw phosphate during heat treatment. High Temperature Materials and Processes 2004;23(3):185-94.

Mohammadi N, Khani H, Gupta VK, Amereh E, Agarwal S. Adsorption process of methyl orange dye onto mesoporous carbon material-kinetic and thermodynamic studies. Journal of Colloid and Interface Science 2011;362:457-62.

Mouflih M, Aklil A, Jahroud N, Gourai M, Sebti S. Removal of lead from aqueous solutions by natural phosphate. Hydrometallurgy 2006;81:219-25.

Nikcevic I, Jokanovic V, Mitric M, Nedic Z, Makovec D, Uskokovic D. Mechanochemical synthesis of nanostructured fluorapatite/fluorhydroxyapatite and carbonated fluorapatite/ fluorhydroxyapatite. Journal of Solid State Chemistry 2004; 177:2565-74.

Pignatello JJ. The measurement and interpretation of sorption and desorption rates for organic compounds in soil media. Advances in Agronomy 1999;69:1-73.

Rytwo G, Ruiz‐Hitzky E. Enthalpies of adsorption of methylene blue and crystal violet to montmorillonite: Enthalpies of adsorption of dyes to montmorillonite. Journal of Thermal Analysis and Calorimetry 2003;71:751-9.

Sabar S, Abdul-Aziz H, Yusof NH, Subramaniam S, Foo KY, Wilson LD, et al. Preparation of sulfonated chitosan for enhanced adsorption of methylene blue from aqueous solution. Reactive and Functional Polymers 2020;151:Article No.104584.

Sadiq M, Abdennouri M, Barka N, Baalala M, Lamonier C, Bensitel M. Influence of the crystal phase of magnesium phosphates catalysts on the skeletal isomerization of 3,3-dimethylbut-1-ene. Canadian Chemical Transactions 2015; 3(2):225-33.

Tóth J. Thermodynamical correctness of gas/solid adsorption isotherm equations. Journal of Colloid and Interface Science 1994;163:299-302.

Tsuda S, Matsusaka N, Madarame H, Ueno S, Susa N, Ishida K, et al. The comet assay in eight mouse organs: Results with 24 azo compounds. Mutation Research/Genetic Toxicology and Environmental Mutagenesis 2000;465(1-2):11-26.

Wang M, Li G, Huang L, Xue J, Liu Q, Bao N, et al. Study of ciprofloxacin adsorption and regeneration of activated carbon prepared from *Enteromorpha prolifera* impregnated with H_3PO_4 and sodium benzenesulfonate. Ecotoxicology and Environmental Safety 2017;139:36-42.

Wang M, Qian R, Bao M, Gu C, Zhu P. Raman, FT-IR and XRD study of bovine bone mineral and carbonated apatites with different carbonate levels. Materials Letters 2018;210:203-6.

Yous R, Mohellebi F, Cherifi H, Amrane A. Competitive biosorption of heavy metals from aqueous solutions onto *Streptomyces rimosus*. Korean Journal of Chemical Engineering 2018;35:890-9.

Zahrani EM, Fathi MH. The effect of high-energy ball milling parameters on the preparation and characterization of fluorapatite nanocrystalline powder. Ceramics International 2009;35:2311-23.